Ab initio calculation of hafnium and zirconium melting curves via the Lindemann criterion

D. V. Minakov,* M. A. Paramonov,† G. S. Demyanov,‡ V. B. Fokin,§ and P. R. Levashov‖
Joint Institute for High Temperatures, Izhorskaya 13 Bldg 2, Moscow 125412, Russia
and Moscow Institute of Physics and Technology, Institutskiy Pereulok 9, Dolgoprudny, Moscow Region 141701, Russia

(Received 23 September 2022; revised 18 November 2022; accepted 21 November 2022; published 12 December 2022)

In this work we present the melting curves of hafnium and zirconium obtained using quantum molecular dynamics calculations. The mean-square displacements computed during *ab initio* simulations of a crystal phase are used to reconstruct the melting curve according to the Lindemann criterion. The resulting Zr melting curve shows a steeper slope in the low-pressure region compared to some recent diamond-anvil cell experiments but agrees with our previous estimate via the Clausius-Clapeyron relation. The slope for higher pressures is consistent with the experimental one. As for Zr, the Hf melting curve also has a similar steep initial slope being in agreement with our estimate from the Clausius-Clapeyron relation. Currently there are no data on the melting of Hf above atmospheric pressure, so we demonstrate the first *ab initio* estimate of the melting curve of Hf up to 225 GPa.

DOI: 10.1103/PhysRevB.106.214105

I. INTRODUCTION

Hafnium (Hf), zirconium (Zr), and titanium (Ti) belong to the same group of the Mendeleev Periodic Table (group IVB). Thus they have a very similar structure of valence electrons; moreover, the chemical properties of hafnium are alike to zirconium [1]. Hafnium is used as a control rod material in nuclear reactors due to its high thermal neutron absorption cross section [2,3]. It also serves as a structural material in water-cooled nuclear reactors since its corrosive resistance turned out to be higher than that of zirconium [3].

For successful and safe use of Zr and Hf in nuclear power engineering, it is necessary to know their thermal properties as well as phase diagrams. At room temperature and atmospheric pressure, Hf exists in the α phase (the hcp crystal structure). When heated, it transforms into the β phase (bcc lattice), which was first reported nearly 100 years ago [4] and studied in detail later [5–7]. Ti and Zr show similar behavior [8], although the transition happens at lower temperatures [9]. The transformation from the α phase to the ω one (hexagonal crystal structure) also occurs at much higher pressures for Hf than for Ti and Zr [9]. In [10], an attempt was made to reproduce the experimental results for Ti, Zr, and Hf crystal structures at zero temperature using density functional theory (DFT). *Ab initio* DFT calculations agree well with the experimental transition pressures [11]. Later, a complete phase diagram of solid Hf was reconstructed in [12,13]. The influence of an exchange-correlation functional as well as the spin-orbit coupling on the phase diagram was considered in [14].

The phonon and elastic properties of Hf are also widely studied. From the theoretical point of view, these properties are considered mostly in the quasiharmonic approximation (QHA) [15]. The phonon dispersion of α-Hf at 295, 800, and 1300 K have been measured in [16,17]. For higher temperatures, the phonon dispersion curves of the β phase of Ti, Zr, and Hf were experimentally determined in [18–20]. As a result of a phonon spectrum calculation, imaginary modes of vibrations in the β phase are observed [13,21–23]; the calculations were performed by "SCAILD" [24] and "small displacement" [25] methods. Thus, the β phase of Ti, Zr, and Hf is dynamically unstable [26] so that the QHA is not suitable in this case and anharmonic effects should be taken into account. Quantum molecular dynamics (QMD) simulations [26] or the "large displacement" method [15] can be used for this purpose; both methods eliminate imaginary modes and provide a better agreement with the experimental phonon spectrum for the β phase. However, the method of Ref. [26] is very computationally expensive, and there is no strict criterion for the amount of displacement in the large displacement approach [15]. In contrast, imaginary modes are not observed for the α phase of Hf, Zr, and Ti [13,27].

Thermophysical properties of pure hafnium were extensively investigated experimentally at very low [28–32] and high temperatures [33,34]. The papers [33,35–38] present information on the enthalpy dependence on temperature, including different aggregate states [36]. Density, heat capacity, surface tension, and viscosity were also reported [34,39–43]. The semiempirical Mie-Grüneisen equation of state (EOS) of Hf was constructed in Ref. [44]; the coefficients were fitted to the data of shock wave experiments. Finally, the multiphase EOS for hafnium [45–47] was constructed, and its critical parameters [48] were estimated.

Both for Hf and Zr, one of the major experimental problems is the avoidance of oxidation which may interfere with reliable transition and melting point determinations and lead to a significant discrepancy in specific heat and enthalpy measured values [37]. A further challenge for hafnium is that nearly all measurements carry out on samples containing zirconium.

*minakovd@ihed.ras.ru
†mikhail.a.paramonov@phystech.edu
‡demyanov.gs@phystech.edu
§vladimir.fokin@phystech.edu
‖pasha@ihed.ras.ru

An extensive review of thermodynamic, transport, and optical properties of Zr, as well as their first-principles calculations, can be found in our previous paper [49]. Using the QMD method we have presented the thermal expansion, enthalpy, electrical resistivity, and normal spectral emissivity of solid and liquid Zr as well as the static structure factor of liquid Zr.

In addition to thermophysical properties, the melting curve, $T_m(P)$, plays an important role in high-pressure technology. Solid Hf and Zr melt from the β phase. As stated above, the anharmonic effects are well known for the β phase of these metals; as a consequence, the QHA is not satisfactory in this case. Thus, the Lindemann criterion based on the QHA and Debye temperature [50] is not applicable to the metals under consideration. Fortunately, the melting curve can be calculated from the Lindemann criterion in its original form [51]. According to this criterion, melting occurs if the amplitude of thermal vibrations exceeds some critical value.

In our work, we perform the first *ab initio* reconstruction of the melting curve of pure hafnium and zirconium by calculating the mean-square displacement (MSD) of ions directly from QMD simulations. At the moment, unlike Zr for which experimental data have recently become available [52–54], Hf melting curve measurements are completely absent. Therefore, to verify the reliability of our method, we present a comparison of the calculated Zr melting curve with experimental data, and then apply the method to Hf.

II. COMPUTATIONAL METHOD

A. Methods used in earlier works

A melting curve can be computed from the modeling of a single phase (solid or liquid) or two phases at once.

The "heat until it melts" (HUM) method is widely used as a single-phase method [55–59]. During the calculation, a computational cell is heated until the entire cell starts to melt. Although this method is not very time-consuming, the resulting melting temperature is usually overestimated and depends on the number of particles, N_{at} (see Sec. IIIC in Ref. [57], Fig. 3 in Ref. [58], and Ref. [59]). It is explained by the overheating of a solid phase [60]: the system becomes metastable so melting may occur at a temperature higher than the equilibrium melting one. The HUM method can be slightly improved using the hysteresis method (see Eq. (1), Fig. 4 in Ref. [58] and Eq. (14) in Ref. [61]).

The Z method is another single-phase simulation approach that appears to yield more accurate results [62–64]. The idea is to perform a long simulation of an overheated solid in the *NVE* ensemble. At some moment, the system should spontaneously melt, causing the temperature to drop to T_m. The major disadvantage of this method is the necessity for a long simulation and a large system [58, Sec. III D]. Previously, an attempt was made to estimate two melting points of Hf at high pressures using the Z method for 432 atoms [65]. However, the theoretical basis of the Z method and its strong dependence on the computational cell size and simulation time are still a matter of debate [66,67].

The two-phase or coexistence method assumes the presence of adjoining solid and liquid phases in the calculation cell [57,68–70]. During the simulation, the interface between the two phases should be at rest. Usually, the resulting melting temperature agrees well with experiment. However, the simulation requires at least a thousand particles to obtain a reliable equilibrium situation so the method is extremely time-consuming especially for the elements with a big number of valence electrons such as hafnium and zirconium.

Based on the two-phase thermodynamic (2PT) model by Lin *et al.* [71] and memory function (MF) formalism, the 2PT-MF technique [72–74] allows one to calculate entropy and free energy via the velocity autocorrelation function. Thus it is possible to compare the Gibbs free energy of two phases to define the melting curve. This method gives results close to the coexistence one for a much lower price. However, the present formulation of the 2PT-MF method has difficulties describing heavy elements.

B. Method of this work

In contrast to the considered above one-phase methods of melting determination the Lindemann criterion [50,51] has a theoretical justification in the case of the inverse power potential $\phi(r) \sim r^{-n}$ [75,76]. It is also known that the Lindemann parameter is almost constant for metals with the same crystal structure (e.g., 0.1–0.13 for fcc metals [77,78]). According to the Lindemann criterion, melting occurs if the amplitude of atom or ion thermal vibrations $\sqrt{\langle u^2(T,P)\rangle}$, depending on temperature T and pressure P, becomes large enough compared to the average interatomic distance:

$$\sqrt{\langle u^2(T_m,P)\rangle} = L_{\text{melt}} d_{at}. \tag{1}$$

Here, $\langle u^2(T,P)\rangle$ is the MSD of ions, L_{melt} is a dimensionless constant and T_m is a melting temperature at pressure P. L_{melt} determines the critical amplitude of thermal vibrations. The notation $L(T,P) = \sqrt{\langle u^2(T,P)\rangle}/d_{at}$ defines the reduced amplitude of vibrations; we refer to it as *the Lindemann parameter*, while the constant L_{melt} will be further referred to as *the critical Lindemann parameter*. The value of the average interatomic distance is calculated as the doubled Wigner-Seitz radius [79, Eq. (19.11)]:

$$d_{at} = \left(\frac{6\Omega}{\pi N_{at}}\right)^{1/3}. \tag{2}$$

It is possible to calculate the MSD using the QHA [78]. In this theory, $\langle u^2(T,P)\rangle$ is determined by the phonon density of states (PhDOS) [80]. The Lindemann criterion (1) with such a choice of $\langle u^2(T,P)\rangle$ showed a very good agreement with experimental data for Al, Cu, and Ni [78,81]. The anharmonicity of vibrations can be accounted for using a thermodynamic integration [82] or machine-learned potentials [83].

Nevertheless, in some cases the quasiharmonic approach cannot be applied. This is valid for metals in which a crystal structure is dynamically unstable at 0 K (i.e., its phonon spectrum contains imaginary frequencies) [26,84]. The same situation may be observed for crystal structures near the melting curve. The anomalous phonon spectra are found, for example, in Li, Zr, and Hf (see Figs. 2, 3 in Ref. [26] and Fig. 7 in Ref. [13]). They can be mended by taking into account the anharmonic contributions to the free energy at elevated

temperatures [15,24,26,85]. However, to restore the meting curve the dependence of PhDOS on temperature and volume is necessary, which requires huge computational costs when using the methods of Refs. [24,26]. On the other hand, in the large displacement approach [15] there is no strict physical criterion for the choice of displacements, which leads to an unsatisfactory dependence of phonon free energy on volume on isotherms.

Therefore, in this work we do not calculate the phonon spectrum at all. Instead, the MSD is calculated directly from the ionic trajectories, and the anharmonic effects are taken into account immediately. A similar method was used in [86]; however, the MSD of ions and the critical Lindemann parameter were estimated with less accuracy.

To calculate the MSD of ions, we perform a QMD simulation in the framework of DFT using the Vienna *Ab initio* Simulation Package (VASP) [87–90]. Next, we briefly describe the simulation method. One may find a more detailed description of the QMD technique in [91].

A simulation is performed in a cubic computational cell for a crystalline system; the *NVT* ensemble is used. The volume of the cell corresponds to a given density ρ; the temperature of ions is maintained via the Nosé thermostat [92]; the same temperature of electrons is set as a parameter in the Fermi-Dirac distribution. After the system reaches equilibrium, we calculate the reference configuration of ions to take into account a possible disruption of the ideal lattice structure in the vicinity of melting. For this purpose, we calculate the equilibrium positions for each ion by averaging its coordinates in all equilibrium configurations. Additionally, we determine the self-diffusion coefficient to make sure that it equals to zero and no irreversible displacements of atoms take place during the equilibrium part of the simulation. Pressure $P = P(T, \rho)$ is determined by averaging of the ionic and electronic contributions over equilibrium configurations.

Then we calculate the MSD with respect to the reference configuration for each equilibrium ion configuration and each ion. These displacements are averaged over all ions and configurations:

$$\langle u^2(T,P)\rangle = \frac{1}{N_{at}N_{cf}} \sum_{c=1}^{N_{cf}} \sum_{i=1}^{N_{at}} \sum_{\alpha=1}^{3} \left(x_{ci}^{\alpha} - x_{ri}^{\alpha}\right)^2, \qquad (3)$$

where T is the simulation temperature, N_{cf} is the number of equilibrium configurations, α stands for the index of the three coordinate axes, x_{ci}^{α} is the α coordinate of ion i in configuration c, and x_{ri}^{α} is the α coordinate of ion i in the reference configuration.

The value of the critical Lindemann parameter L_{melt} depends on the material. To compute it, we perform several simulations at a given temperature T_{m0} corresponding to the reference melting temperature at atmospheric pressure and different densities to obtain the dependence $L(T_{m0}, P)$ on pressure P (see Fig. 1). Then, this dependence is extrapolated to zero pressure to obtain L_{melt}.

To calculate the melting curve, $T_m(P)$, we use Eq. (1). We choose several densities corresponding to a compressed crystalline state. For each density ρ_g (the index g stands for "given"), we perform the simulations at different temperatures to calculate $P(T, \rho_g)$, $L(T, P(T, \rho_g))$. We approximate

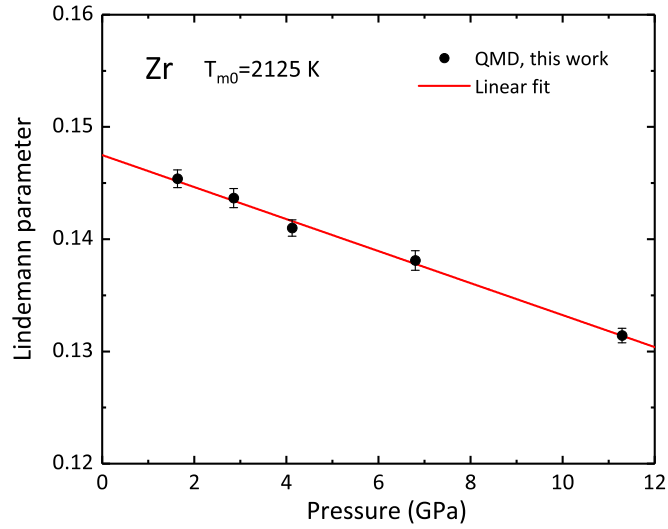

FIG. 1. Determination of the critical Lindemann parameter L_{melt} for Zr. Each point corresponds to a Lindemann parameter $L(T_{m0}, P)$ for the experimental melting temperature $T_{m0} = 2125$ K. This pressure dependence is linearly extrapolated to zero pressure to obtain $L_{\text{melt}} = 0.1475(4) \approx 0.148$.

$P(T, \rho_g)$, $L(T, P(T, \rho_g))$ by linear functions of T; the fitting value $L(T_m, P_m) = L_{\text{melt}}$ corresponds to the melting temperature T_m at a pressure $P_m = P(T_m, \rho_g)$ (see Fig. 2). The melting curve obtained in this way can be fitted by the Simon-Kechin approximation [93, Eq. (13)]:

$$T_m(P) = T_{m0}\left(1 + \frac{P}{A}\right)^B \exp(-C \times P). \qquad (4)$$

We found that the Simon-Kechin approximation describes our melting curve better than the Simon-Glatzel one especially in the low-pressure region, where the slope of the calculated curve changes significantly, as will be demonstrated below.

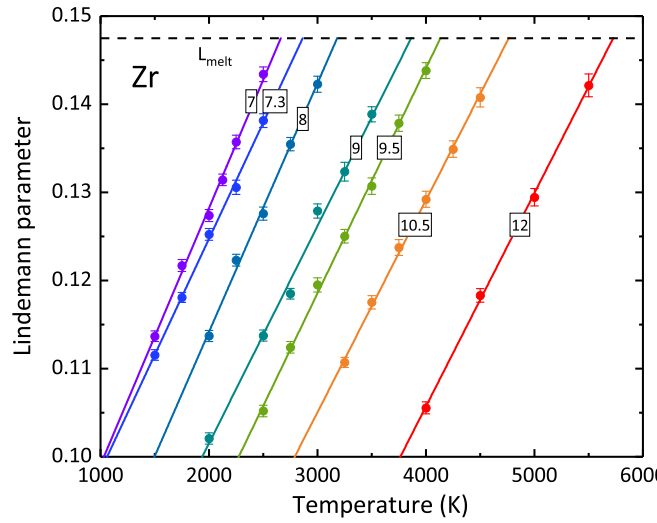

FIG. 2. The temperature dependence of the Lindemann parameter at fixed densities ρ_g for Zr. Points correspond to $L(T, P(T, \rho_g))$ at each density ρ_g. Each dependence $L(T, P(T, \rho_g))$ for a fixed ρ_g is linearly fitted. The substance density, ρ_g, is indicated on every line in g/cm^3. The critical parameter $L_{\text{melt}} \approx 0.148$.

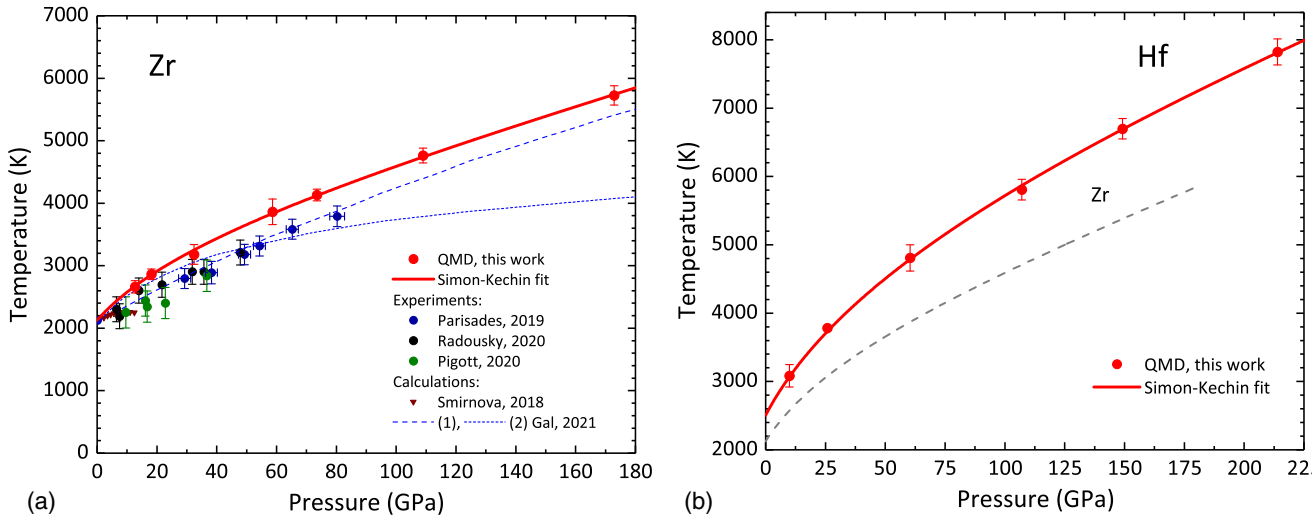

FIG. 3. The melting curve of (a) Zr; (b) Hf. (a) The experimental data for Zr are from [52–54]. The calculation by Smirnova *et al.* [94] is provided via classical molecular dynamics up to 13 GPa. The long-dashed and short-dashed lines from [95] represent the fitted data from Birch-Murnaghan EOS and QMD data of [96], respectively, via the Lindemann-Gilvarry approximation. The red circles and red solid line represent our computational result and Simon-Kechin fit (4), respectively (see Table I). (b) Melting curve of Hf according to our calculations. Our Zr melting curve is shown as a gray dashed curve for comparison.

As can be seen, a reference melting point T_{m0} is needed to obtain L_{melt}. In our work, the experimental value of the melting point at atmospheric pressure is used. However, if necessary, this temperature can be obtained from the methods described above (e.g., by the coexistence method).

III. SIMULATION PARAMETERS

The initial computational cell contains 128 atoms of Zr or Hf in bcc positions, which corresponds to 4^3 unit cells of a bcc lattice. The periodic boundary conditions are imposed. A QMD simulation is performed for no less than 6000 steps with a 2 fs time step. The first 2000 configurations were discarded; the rest of the configurations correspond to the equilibrium section.

During the electronic structure calculation, we use the Perdew-Burke-Ernzerhof (PBE) parametrization [97] for the generalized gradient approximation (GGA) of the exchange-correlation functional. The projector augmented-wave [98] pseudopotentials with 12 valence electrons for both metals are used. A cutoff energy for the plane-wave basis is equal to 500 eV for both Zr and Hf. The Baldereschi mean-value **k** point {1/4, 1/4, 1/4} is used to approximate the Brillouin zone. All bands with occupation numbers greater than 10^{-6} are taken into account during the simulation.

The convergence on the number of atoms and the influence of exchange-correlation functional on the reconstruction of the melting curve are discussed in the Appendix.

IV. RESULTS AND DISCUSSIONS

A. Melting curve of Zr

Since there is no experimental data on the melting curve of hafnium, we verify the presented method by example of Zr. There are several recent experiments [52–54] as well as calculations [94,95] of $T_m(P)$ for Zr. The experimental data [52–54] are obtained with the laser heated diamond-anvil cell (LHDAC) technique. Our calculations using the Lindemann criterion (1) are shown in Fig. 3(a) by red circles. We fitted our data with the Simon-Kechin approximation (4) with $A = 11.7647$ GPa, $B = 0.2965$, and $C = -1.03 \times 10^{-3}$ GPa^{-1}. Our QMD data on the melting curve of Zr are collected in Table I.

As can be seen, our calculations predict a steep slope of the melting curve in the initial pressure range up to 40 GPa. At higher pressures the slope becomes flatter. We can note that our curve is consistent with the measurements by Radousky *et al.* [53] up to 20 GPa. As for higher pressures, all available experimental data [52–54] are slightly lower than our curve;

TABLE I. Melting curve data for Zr and Hf based on our QMD calculations. σ_{T_m} is a statistical error of temperature and ρ_g is the density of the solid phase at melting.

T_m (K)	σ_{T_m} (K)	P_m (GPa)	ρ_g (g/ cm^3)
	Zr		
2662	99	12.7	7.0
2864	84	18.2	7.3
3181	157	32.4	8.0
3863	205	58.6	9.0
4133	93	73.5	9.5
4763	117	109.0	10.5
5726	153	172.8	12.0
	Hf		
3083	165	9.9	13.50
3782	27	25.8	15.00
4808	192	60.4	17.55
5806	151	107.0	20.12
6698	150	149.1	21.95
7822	191	214.0	24.31

however, the slope matches that of Parisiades *et al.* [52] and Gal [95] (long-dashed curve). It should be noted that the slope of our calculated curve at zero pressure $dT_m/dP \approx 56$ K/GPa is consistent with the one obtained via the Clausius-Clapeyron relation ($dT_m/dP = T_{m0}\Delta V_{\rm fus}/\Delta H_{\rm fus} \approx 60$ K/GPa) using the enthalpy of fusion $\Delta H_{\rm fus} \approx 14$ kJ/mol and volume change $\Delta V_{\rm fus}/V_{\rm solid} \approx 2.6\%$ for Zr at melting calculated in our previous work [49]. Here, $V_{\rm solid}$ is the volume of the solid phase at $T = T_{m0}$.

As has been shown in our previous work [78] and confirmed in [81], the calculated Ni melting curve is located higher than that obtained in LHDAC experiments up to 2013 [109–111]. Later experiments [112,113], however, agree quite well with our melting curve from Ref. [78]. The underestimation of melting curves in LHDAC experiments as well as challenges due to uncertainties in the material's emissivity, thermal gradients, and other experimental factors are discussed in detail by Hrubiak *et al.* [114] by example of molybdenum. A systematic underestimation of LHDAC melting data compared to shock wave experiments and theoretical predictions is clearly observed for iron [115]. It is possible that the melting curve of Zr in Refs. [52–54] may also be slightly underestimated.

In [95] the melting curve of Zr was evaluated. It was calculated with the Lindemann-Gilvarry criterion [50] based on QMD simulations from [96]. The result [95, Fig. 2] appears to be frustrating [see also Fig. 3(a), the blue short-dashed line]. The author of [95] concludes that "the mismatch demonstrates the difficulties of the DFT theory to predict melting curves." We are strongly opposed to such a statement. The calculation of the melting curve in [95] from QMD data [96] is done using the Lindemann-Gilvarry approximation, which is based upon the quasiharmonic theory. Due to strong anharmonic effects in the bcc phase of Zr such an approach can lead to significant errors.

We can repeat here that DFT data and the Lindemann criterion have previously provided excellent agreement with experimental data for better studied metals [78,86,116].

B. Melting curve of Hf

Our estimation of the Hf melting curve is presented in Fig. 3(b) together with the melting curve of Zr for comparison. The determination of the critical Lindemann parameter $L_{\rm melt}$ for Hf is shown in Fig. 4(a). The corresponding value $L_{\rm melt} = 0.1594(2) \approx 0.16$ was obtained through the linear extrapolation of calculated parameters along the isotherm $T_{m0} = 2506$ K to zero pressure. Six isochors referring to the densities ρ_g were computed to reconstruct the melting curve up to 225 GPa (see Table I). The temperature dependencies of the Lindemann parameter along the isochores were linearly fitted and extrapolated to $L_{\rm melt}$ as shown in Fig. 4(b). The pressure values for the melting curve were determined using linear approximations for the calculated $P - T$ dependencies along the isochores. The obtained result is well fitted via the Simon-Kechin relation with parameters $A = 14.2857$ GPa, $B = 0.3745$, and $C = -4.6341 \times 10^{-4}$ GPa^{-1}. QMD data on the Hf melting curve are collected in Table I.

As can be seen from Fig. 3(b) our calculated Hf melting curve has a steep slope at $P = 0$ ($dT_m/dP \approx 67$ K/GPa), as in

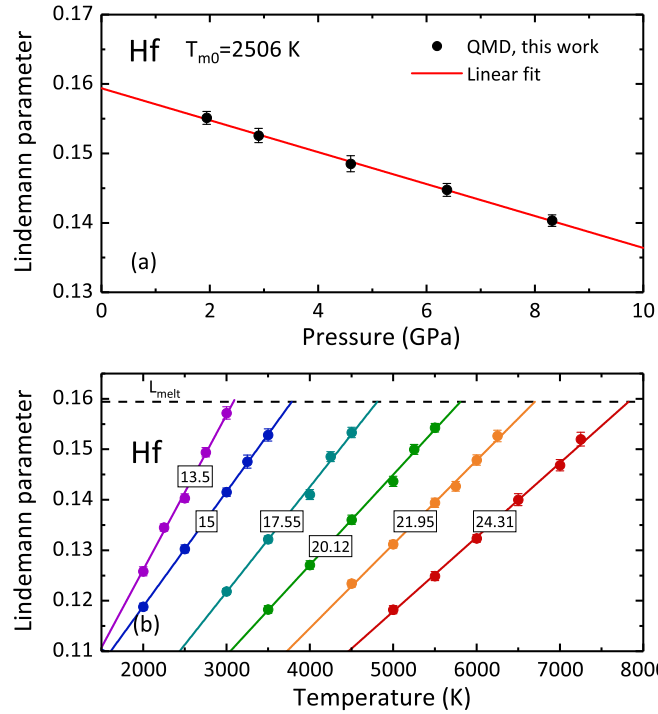

FIG. 4. Lindemann parameter along the isotherm $T_{m0} = 2506$ K and isochors for Hf. (a) Linear extrapolation of calculated $L(T_{m0}, P)$ to zero pressure gives a critical Lindemann parameter $L_{\rm melt} = 0.1594(2) \approx 0.16$. (b) The temperature dependence of the Lindemann parameter at fixed densities. Points correspond to $L(T, P(T, \rho_g))$ at some (T, ρ_g). Each temperature dependence of $L(T, P(T, \rho_g))$ for a fixed ρ_g is linearly fitted. The density is indicated on every line in g/cm^3. The critical Lindemann parameter $L_{\rm melt} \approx 0.16$.

case of Zr. To prove this conclusion, we decided to reconstruct the isobaric expansion (IEX) curve in the vicinity of melting for solid and liquid Hf to estimate the slope of the melting curve via the Clausius-Clapeyron relation. We performed a series of calculations along isochores in the liquid phase and along isotherms in the solid phase. A larger number of atoms (250) were used in these simulations to ensure the convergence of thermodynamic properties (i.e., pressure error of less than 1 kbar) in the vicinity of melting. Then the calculated points were interpolated by a quadratic polynomial or a linear fit, and the interpolation relations were used to restore the zero isobar. This approach helps to reduce the influence of computational errors and allows the IEX curve to be reconstructed with high accuracy at a given pressure, as demonstrated earlier for Mo [117,118], Re [119], and Zr [49].

Our reconstructed IEX curve in the density vs temperature plot is presented in Fig. 5 as well as available experimental measurements and some theoretical predictions. Our results are in very good agreement with electrostatic levitation (ESL) data by Paradis [40] both for solid and liquid Hf, as well as with ESL data by Yoo *et al.* [42] for liquid Hf. The density of molten Hf measured at T_m by Ivashchenko and Martsenyuk [99] and calculated by Allen [101] is also consistent with our prediction. It should be noted that our QMD-calculated isobar for liquid Hf perfectly agrees with the prediction by Steinberg

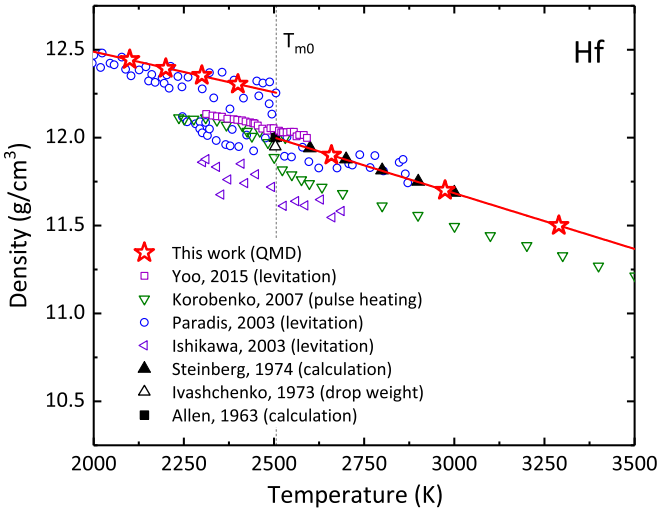

FIG. 5. Isobaric expansion of solid and liquid Hf in the density versus temperature diagram. Star symbols are QMD data; red lines are linear approximations. Experimental isobaric data: pulse heating [43] is green down triangles; electrostatic levitation measurements [39,40,42] are blue open circles, left violet triangles, and open purple squares, correspondingly. Molten density measurement [99] is black open triangle. Density calculations of liquid Hf [100,101] are black solid triangles and square.

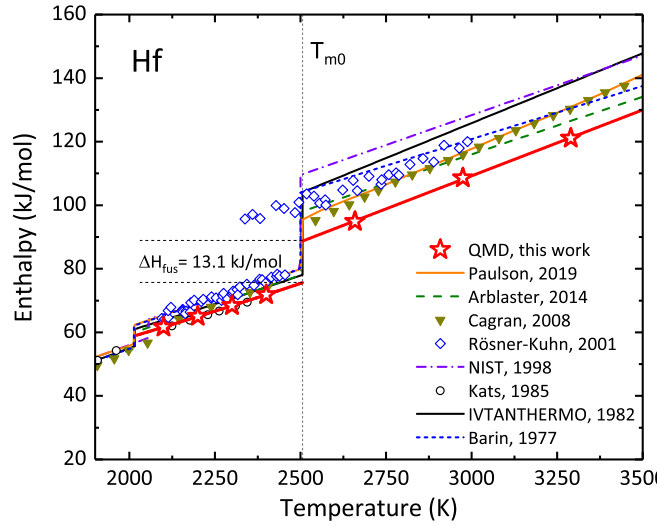

FIG. 6. Molar enthalpy versus temperature for Hf. Star symbols are QMD data; red lines are approximations. Experimental data [33,102,103] are shown as symbols. Orange solid line is the relation by Paulson *et al.* [104] obtained using the Bayesian framework for a selection of experimental data, the relation by Arblaster [37] is a green dashed line, the relation from Thermochemical Table NIST [105] is a violet dash-dotted line, the blue dashed line is the data from the handbook of thermochemical properties of inorganic substances by Barin *et al.* [106], and the black line is the approximation from the IVTANTHERMO handbook [107,108].

[100] made using the similarity law. Meanwhile, the pulse heating experimental data by Korobenko and Savvatimskii [43] have a similar slope of the thermal expansion curve but predict lower density for liquid Hf. It may be noted that the volume expansion measurements seem to be the most challenging task of the IEX experiments with pulse heating. Both the capabilities and features of experimental instruments and the complexity of the accompanying physical phenomena may prevent obtaining reliable data on the dependence of density on temperature [120].

Molar enthalpy for solid and liquid Hf in the vicinity of melting is plotted versus temperature in Fig. 6. Our calculations agree very well with experimental and reference data for β-Hf; the best agreement is observed for the enthalpy measurements by Kats [103] and Cagran *et al.* [102]. On the other hand, for liquid Hf QMD predicts significantly lower enthalpy than can be found in NIST [105], IVTANTHERMO [107,108], and Barin's handbook [106], and recent reviews [37,104] and experiments [33,102]. Nevertheless, the slope of our molar enthalpy curve, which by definition is isobaric heat capacity, for liquid Hf is close to that from the IVTANTHERMO handbook and Rösner-Kuhn *et al.* Our calculations predict $C_p \approx 41.5$ J mol^{-1} K^{-1} for liquid Hf, IVTANTHERMO, 44; Rösner-Kuhn *et al.* [33], 40; Korobenko *et al.* [34], 42.8; and Paulson *et al.* [104], 45 J $\times$ mol^{-1} K^{-1}. Meanwhile, the figure shows that there is a strong discrepancy between the measurements for liquid Hf, mainly due to different estimates of the melting enthalpy jump, which differs almost twice from 14.69 [102] to 29 kJ/mol [105]. Our QMD calculations predict the lowest value of the enthalpy of fusion among available estimates of about 13.1 kJ/mol. For comparison, the lowest measured values of the enthalpy of fusion for Hf were presented by Cagran *et al.* [102], 14.69; by Paradis *et al.* [40], 15.1; by Kang *et al.* [121], 15.68; and by Korobenko *et al.* [34], 16.06 kJ/mol. At the same time, it should be mentioned here, that experimental samples of Hf usually consist of about 3 mass % of Zr so the influence of the impurities on the thermophysical properties may be significant. For example, when corrected by the Kopp-Neumann rule the enthalpy of fusion by Paradis *et al.* can be refined downward to 14.62 kJ/mol [37].

To sum up, our QMD calculations for Hf predict a substantial volume change on melting $\Delta V_{\rm fus} = 1.7567 \times 10^{-3}$ cm^3/g or about 2.15% volume jump in agreement with ESL experiments and at the same time the lowest value of the enthalpy of fusion ($\Delta H_{\rm fus} \approx 13.1$ kJ/mol). This leads to a steep slope of the melting curve at $P = 0$ of $dT_m/dP \approx 60$ K/GPa via the Clausius-Clapeyron relation, that is consistent with our estimate via the Lindemann criterion.

V. CONCLUSION

The famous Lindemann criterion [51] appeared more than 100 years ago and has been proving its usefulness in numerous publications. Having a theoretical justification for an inverse power potential, it works very well in many practical situations. The Gilvarry reformulation of the criterion [50] connects melting with the Debye temperature and Grüneisen parameter. In this form the Lindemann criterion is widely used to predict melting as all necessary information for the calculation is available from the QHA. However, in the case of Zr and Hf the QHA fails due to strong anharmonic effects in the bcc structure of these metals. The criterion still can be used, but

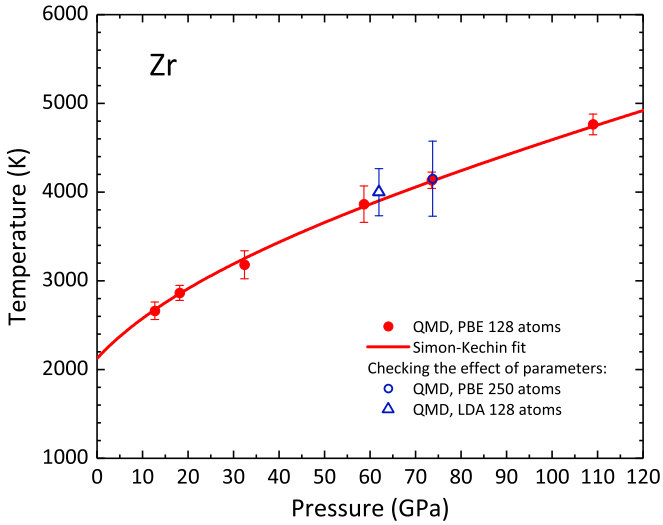

FIG. 7. Melting curve of Zr from QMD simulations and the Lindemann criterion. Red solid circles correspond to 128 atoms and the GGA-PBE exchange-correlation functional, the blue open circle is for the GGA-PBE and 250 atoms, and the blue triangle is for the LDA-CA and 128 atoms.

the amplitude of ionic vibrations should be calculated directly from molecular dynamics simulations.

In this work we apply the QMD method to calculate the MSD of ions and restore the melting curves of Zr and Hf using the Lindemann criterion in its original form. We accurately determine the reference configuration and study ionic vibrations with respect to it. The critical Lindemann parameter is obtained by extrapolation of the Lindemann parameter at the reference melting temperature to zero pressure. Then the melting curve is calculated by extrapolation of the Lindemann parameter on different isochores to the critical value. We obtained the following values of the critical Lindemann parameter: $L_{\text{melt}} = 0.148$ for Zr and $L_{\text{melt}} = 0.16$ for Hf. The melting curves for both metals show a rather steep slope at $P = 0$, which becomes flatter at higher pressures. Independently, we calculated the initial slope of the melting curves from the Clausius-Clapeyron relation for Zr [49] and revealed good correspondence with the Lindemann criterion. To make a similar checkout for Hf we calculated the IEX curve to obtain the values of $\Delta H_{\text{fus}} \approx 13.1$ kJ/mol and $\Delta V_{\text{fus}}/V_{\text{solid}} \approx 2.15\%$. The enthalpy of fusion for Hf turned out to be the lowest among other values while the volume jump was in agreement with ESL experiments. Nevertheless, the slope of the Hf melting curve at $P = 0$ from the Clausius-Clapeyron relation is close to that from the Lindemann criterion. Thus, the first *ab initio* melting curves for Hf and Zr are obtained. Unlike many similar works, we also present the density of solid phase at melting for both metals.

ACKNOWLEDGMENTS

The authors acknowledge the JIHT RAS Supercomputer Centre, the Joint Supercomputer Centre of the Russian Academy of Sciences, and the Shared Resource Centre Far Eastern Computing Resource IACP FEB RAS for providing computing time. The work was supported by Rosatom (Contract No. 1770641334821000139O/226/3468-D).

APPENDIX: INFLUENCE OF SIMULATION PARAMETERS ON MELTING CURVE RECONSTRUCTION

We checked the reliability of our calculation of the melting curve of Zr by performing additional calculations with more atoms in a supercell and with another exchange-correlation functional. The results of these tests for 250 atoms and for the LDA-CA [122] exchange-correlation functional are shown in Fig. 7. For both cases we redefined the critical Lindemann parameter by calculating the isotherm $T_m = 2125$ K with the alternative simulation parameters. As can be seen from the figure, the predicted melting temperature remains the same within the error bars even for different exchange-correlation functionals.

[1] R. H. Nielsen, updated by staff, Hafnium and Hafnium Compounds, in *Kirk-Othmer Encyclopedia of Chemical Technology* (Wiley, New York, 2013), pp. 1–19.

[2] A. I. Savvatimskiy and S. V. Onufriev, Method and apparatus for studying high-temperature properties of conductive materials in the interests of nuclear power engineering, Phys. At. Nucl. **79**, 1637 (2016).

[3] S. K. Dutta and D. R. Lodhari, *Extraction of Nuclear and Non-Ferrous Metals* (Springer, Singapore, 2018).

[4] C. Zwikker, Transitions in zirconium and hafnium, Physica **6**, 361 (1926).

[5] P. Duwez, The allotropic transformation of hafnium, J. Appl. Phys. **22**, 1174 (1951).

[6] J. D. Fast, The allotropic transformation of hafnium and a tentative equilibrium diagram of the system zirconium-hafnium, J. Appl. Phys. **23**, 350 (1952).

[7] J. C. Jamieson, Crystal structures of titanium, zirconium, and hafnium at high pressures, Science **140**, 72 (1963).

[8] E. S. Fisher and C. J. Renken, Single-Crystal Elastic Moduli and the hcp → bcc Transformation in Ti, Zr, and Hf, Phys. Rev. **135**, A482 (1964).

[9] H. Xia, G. Parthasarathy, H. Luo, Y. K. Vohra, and A. L. Ruoff, Crystal structures of group IVa metals at ultrahigh pressures, Phys. Rev. B **42**, 6736 (1990).

[10] R. Ahuja, J. M. Wills, B. Johansson, and O. Eriksson, Crystal structures of Ti, Zr, and Hf under compression: Theory, Phys. Rev. B **48**, 16269 (1993).

[11] G. Jomard, L. Magaud, and A. Pasturel, Full-potential calculations using the generalized-gradient corrections: Structural properties of Ti, Zr and Hf under compression, Philos. Mag. B **77**, 67 (1998).

[12] S. Ostanin and V. Trubitsin, Calculation of the $\mathcal{P}$–$\mathcal{T}$ phase diagram of hafnium, Comput. Mater. Sci. **17**, 174 (2000).

[13] C.-B. Zhang, W.-D. Li, P. Zhang, and B.-T. Wang, First-principles calculations of phase transition, elasticity, phonon

spectra, and thermodynamic properties for hafnium, Comput. Mater. Sci. **157**, 121 (2019).
[14] H. Fang, M. Gu, B. Liu, X. Liu, S. Huang, C. Ni, Z. Li, and R. Wang, Plane-wave pseudopotential study for the structural stability of Hf: The role of spin–orbit interaction, Phys. B: Condens. Matter **406**, 1744 (2011).
[15] N. Antolin, O. D. Restrepo, and W. Windl, Fast free-energy calculations for unstable high-temperature phases, Phys. Rev. B **86**, 054119 (2012).
[16] C. Stassis, D. Arch, O. D. McMasters, and B. N. Harmon, Lattice dynamics of hcp Hf, Phys. Rev. B **24**, 730 (1981).
[17] C. Stassis, D. Arch, J. Zarestky, O. McMasters, and B. Harmon, On the lattice dynamics of hcp hafnium, Solid State Commun. **35**, 259 (1980).
[18] W. Petry, A. Heiming, J. Trampenau, M. Alba, C. Herzig, H. R. Schober, and G. Vogl, Phonon dispersion of the bcc phase of group-IV metals. I. bcc titanium, Phys. Rev. B **43**, 10933 (1991).
[19] A. Heiming, W. Petry, J. Trampenau, M. Alba, C. Herzig, H. R. Schober, and G. Vogl, Phonon dispersion of the bcc phase of group-IV metals. II. bcc zirconium, a model case of dynamical precursors of martensitic transitions, Phys. Rev. B **43**, 10948 (1991).
[20] J. Trampenau, A. Heiming, W. Petry, M. Alba, C. Herzig, W. Miekeley, and H. R. Schober, Phonon dispersion of the bcc phase of group-IV metals. III. bcc hafnium, Phys. Rev. B **43**, 10963 (1991).
[21] K. Persson, M. Ekman, and V. Ozoliņš, Phonon instabilities in bcc Sc, Ti, La, and Hf, Phys. Rev. B **61**, 11221 (2000).
[22] P. Souvatzis, O. Eriksson, M. I. Katsnelson, and S. P. Rudin, Entropy Driven Stabilization of Energetically Unstable Crystal Structures Explained from First Principles Theory, Phys. Rev. Lett. **100**, 095901 (2008).
[23] C.-E. Hu, Z.-Y. Zeng, L. Zhang, X.-R. Chen, L.-C. Cai, and D. Alfè, Theoretical investigation of the high pressure structure, lattice dynamics, phase transition, and thermal equation of state of titanium metal, J. Appl. Phys. **107**, 093509 (2010).
[24] P. Souvatzis, O. Eriksson, M. I. Katsnelson, and S. P. Rudin, The self-consistent *ab initio* lattice dynamical method, Comput. Mater. Sci. **44**, 888 (2009).
[25] D. Alfè, PHON: A program to calculate phonons using the small displacement method, Comput. Phys. Commun. **180**, 2622 (2009).
[26] O. Hellman, I. A. Abrikosov, and S. I. Simak, Lattice dynamics of anharmonic solids from first principles, Phys. Rev. B **84**, 180301(R) (2011).
[27] W. Sun, W. Luo, Q. Feng, and R. Ahuja, Anisotropic distortion and Lifshitz transition in α-Hf under pressure, Phys. Rev. B **95**, 115130 (2017).
[28] S. Cristescu and F. Simon, Die spezifischen Wärmen von beryllium, germanium und hafnium bei tiefen temperaturen, Z. Phys. Chem. **25B**, 273 (1934).
[29] N. M. Wolcott, The atomic heats of titanium, zirconium and hafnium, Philos. Mag. **2**, 1246 (1957).
[30] G. D. Kneip, J. O. Betterton, and J. O. Scarbrough, Low-Temperature Specific Heats of Titanium, Zirconium, and Hafnium, Phys. Rev. **130**, 1687 (1963).
[31] E. W. Collings and J. C. Ho, Magnetic-susceptibility and low-temperature specific-heat studies of Ti, Zr, and Hf, Phys. Rev. B **4**, 349 (1971).
[32] I. O. Bashkin, M. V. Nefedova, V. G. Tissen, and E. G. Ponyatovsky, Superconducting transition temperature in hafnium under pressures up to 64 GPa, J. Exp. Theor. Phys. Lett. **80**, 655 (2004).
[33] M. Rösner-Kuhn, K. Drewes, H. Franz, and M. G. Frohberg, Enthalpy measurements of the solid high-temperature β-phase and the liquid phase of hafnium (3 wt. % Zr) by levitation drop calorimetry, Mater. Sci. Eng.: A **308**, 60 (2001).
[34] V. N. Korobenko, O. A. Polyakova, and A. I. Savvatimskii, Heat capacity of liquid hafnium from the melting point to the boiling point at atmospheric pressure, High Temp. **43**, 38 (2005).
[35] D. T. Hawkins, M. Onillon, and R. L. Orr, High-temperature heat content of hafnium, J. Chem. Eng. Data **8**, 628 (1963).
[36] R. Ackermann and E. Rauh, The thermodynamics and vaporization of thorium, hafnium, and zirconium, J. Chem. Thermodyn. **4**, 521 (1972).
[37] J. W. Arblaster, Thermodynamic properties of hafnium, J. Phase Equilib. Diffus. **35**, 490 (2014).
[38] S. V. Onufriev, V. A. Petukhov, V. R. Pesochin, and V. D. Tarasov, The thermophysical properties of hafnium in the temperature range from 293 to 2000 K, High Temp. **46**, 203 (2008).
[39] T. Ishikawa, P.-F. Paradis, T. Itami, and S. Yoda, Thermophysical properties of liquid refractory metals: Comparison between hard sphere model calculation and electrostatic levitation measurements, J. Chem. Phys. **118**, 7912 (2003).
[40] P.-F. Paradis, T. Ishikawa, and S. Yoda, Non-contact measurements of the thermophysical properties of hafnium-3 mass% zirconium at high temperature, Int. J. Thermophys. **24**, 239 (2003).
[41] Y. Sun, H. Muta, and Y. Ohishi, Heat capacity of liquid transition metals obtained with aerodynamic levitation, J. Chem. Thermodyn. **171**, 106801 (2022).
[42] H. Yoo, C. Park, S. Jeon, S. Lee, and G. W. Lee, Uncertainty evaluation for density measurements of molten Ni, Zr, Nb and Hf by using a containerless method, Metrologia **52**, 677 (2015).
[43] V. N. Korobenko and A. I. Savvatimskii, The density of liquid hafnium from the melting point to the boiling point, High Temp. **45**, 159 (2007).
[44] W. H. Gust and E. B. Royce, New electronic interactions in rare-earth metals at high pressure, Phys. Rev. B **8**, 3595 (1973).
[45] I. V. Lomonosov, Phase diagrams and thermodynamic properties of metals at high pressures and temperatures (in Russian), Sc. D. thesis, Institute of Problems of Chemical Physics, 2000.
[46] R. Hrubiak, V. Drozd, A. Karbasi, and S. K. Saxena, High P-T phase transitions and P-V-T equation of state of hafnium, J. Appl. Phys. **111**, 112612 (2012).
[47] L. Q. Huston, N. Velisavljevic, J. S. Smith, G. T. Gray, and B. T. Sturtevant, Multi-phase equation of state of ultrapure hafnium to 120 GPa, J. Phys.: Condens. Matter **34**, 055401 (2022).
[48] S. V. Onufriev, Estimation of zirconium, hafnium, and tungsten critical parameters, High Temp. **49**, 205 (2011).
[49] M. A. Paramonov, D. V. Minakov, V. B. Fokin, D. V. Knyazev, G. S. Demyanov, and P. R. Levashov, *Ab initio* inspection of thermophysical experiments for zirconium near melting, J. Appl. Phys. **132**, 065102 (2022).

[50] J. J. Gilvarry, The Lindemann and Grüneisen Laws, Phys. Rev. **102**, 308 (1956).

[51] F. A. Lindemann, The calculation of molecular vibration frequencies, Phys. Z. **11**, 609 (1910).

[52] P. Parisiades, F. Cova, and G. Garbarino, Melting curve of elemental zirconium, Phys. Rev. B **100**, 054102 (2019).

[53] H. B. Radousky, M. R. Armstrong, R. A. Austin, E. Stavrou, S. Brown, A. A. Chernov, A. E. Gleason, E. Granados, P. Grivickas, N. Holtgrewe, H. J. Lee, S. S. Lobanov, B. Nagler, I. Nam, V. Prakapenka, C. Prescher, P. Walter, A. F. Goncharov, and J. L. Belof, Melting and refreezing of zirconium observed using ultrafast x-ray diffraction, Phys. Rev. Res. **2**, 013192 (2020).

[54] J. S. Pigott, N. Velisavljevic, E. K. Moss, N. Draganic, M. K. Jacobsen, Y. Meng, R. Hrubiak, and B. T. Sturtevant, Experimental melting curve of zirconium metal to 37 GPa, J. Phys.: Condens. Matter **32**, 355402 (2020).

[55] J.-Y. Raty, E. Schwegler, and S. A. Bonev, Electronic and structural transitions in dense liquid sodium, Nature (London) **449**, 448 (2007).

[56] F. Cricchio, A. B. Belonoshko, L. Burakovsky, D. L. Preston, and R. Ahuja, High-pressure melting of lead, Phys. Rev. B **73**, 140103(R) (2006).

[57] A. B. Belonoshko, R. Ahuja, O. Eriksson, and B. Johansson, Quasi *ab initio* molecular dynamic study of Cu melting, Phys. Rev. B **61**, 3838 (2000).

[58] J. Bouchet, F. Bottin, G. Jomard, and G. Zérah, Melting curve of aluminum up to 300 GPa obtained through *ab initio* molecular dynamics simulations, Phys. Rev. B **80**, 094102 (2009).

[59] A. B. Belonoshko, R. Ahuja, and B. Johansson, Quasi–*Ab Initio* Molecular Dynamic Study of Fe Melting, Phys. Rev. Lett. **84**, 3638 (2000).

[60] A. B. Belonoshko, S. I. Simak, A. E. Kochetov, B. Johansson, L. Burakovsky, and D. L. Preston, High-Pressure Melting of Molybdenum, Phys. Rev. Lett. **92**, 195701 (2004).

[61] S.-N. Luo, A. Strachan, and D. C. Swift, Nonequilibrium melting and crystallization of a model Lennard-Jones system, J. Chem. Phys. **120**, 11640 (2004).

[62] A. B. Belonoshko, N. V. Skorodumova, A. Rosengren, and B. Johansson, Melting and critical superheating, Phys. Rev. B **73**, 012201 (2006).

[63] S. Wang, G. Zhang, H. Liu, and H. Song, Modified Z method to calculate melting curve by molecular dynamics, J. Chem. Phys. **138**, 134101 (2013).

[64] A. B. Belonoshko and A. Rosengren, High-pressure melting curve of platinum from *ab initio* Z method, Phys. Rev. B **85**, 174104 (2012).

[65] L. Burakovsky, N. Burakovsky, D. Preston, and S. Simak, Systematics of the third row transition metal melting: The HCP metals rhenium and osmium, Crystals **8**, 243 (2018).

[66] D. Alfè, C. Cazorla, and M. J. Gillan, The kinetics of homogeneous melting beyond the limit of superheating, J. Chem. Phys. **135**, 024102 (2011).

[67] L.-F. Zhu, B. Grabowski, and J. Neugebauer, Efficient approach to compute melting properties fully from *ab initio* with application to Cu, Phys. Rev. B **96**, 224202 (2017).

[68] A. Ladd and L. Woodcock, Interfacial and co-existence properties of the Lennard-Jones system at the triple point, Mol. Phys. **36**, 611 (1978).

[69] T. Ogitsu, E. Schwegler, F. Gygi, and G. Galli, Melting of Lithium Hydride under Pressure, Phys. Rev. Lett. **91**, 175502 (2003).

[70] D. Alfè, First-principles simulations of direct coexistence of solid and liquid aluminum, Phys. Rev. B **68**, 064423 (2003).

[71] S.-T. Lin, M. Blanco, and W. A. Goddard, The two-phase model for calculating thermodynamic properties of liquids from molecular dynamics: Validation for the phase diagram of Lennard-Jones fluids, J. Chem. Phys. **119**, 11792 (2003).

[72] M. P. Desjarlais, First-principles calculation of entropy for liquid metals, Phys. Rev. E **88**, 062145 (2013).

[73] G. Robert, P. Legrand, P. Arnault, N. Desbiens, and J. Clérouin, Simple calculation of *ab initio* melting curves: Application to aluminum, Phys. Rev. E **91**, 033310 (2015).

[74] D. Minakov, P. Levashov, and V. Fokin, Vibrational spectrum and entropy in simulation of melting, Comput. Mater. Sci. **127**, 42 (2017).

[75] W. G. Hoover and M. Ross, Statistical theories of melting, Contemp. Phys. **12**, 339 (1971).

[76] S. M. Stishov, The thermodynamics of melting of simple substances, Sov.et Phys. Usp. **17**, 625 (1975).

[77] G. Grimvall, Characteristic quantities and dimensional analysis, Sci. Model. Simul. **15**, 21 (2008).

[78] D. V. Minakov and P. R. Levashov, Melting curves of metals with excited electrons in the quasiharmonic approximation, Phys. Rev. B **92**, 224102 (2015).

[79] G. Grimvall, Estimations and correlations, in *Thermophysical Properties of Materials*, edited by G. Grimvall (Elsevier Science B.V., Amsterdam, 1999), Chap. 19, pp. 331–352.

[80] T. Yildirim and A. B. Harris, Lattice dynamics of solid C_{60}, Phys. Rev. B **46**, 7878 (1992).

[81] N. Quang Hoc, T. Dinh Cuong, B. Duc Tinh, and L. Hong Viet, High-pressure melting curves of FCC metals Ni, Pd and Pt with defects, Mod. Phys. Lett. B **33**, 1950300 (2019).

[82] L. Vočadlo and D. Alfè, *Ab initio* melting curve of the fcc phase of aluminum, Phys. Rev. B **65**, 214105 (2002).

[83] Y. Zhou, P. Srinivasan, F. Körmann, B. Grabowski, R. Smith, P. Goddard, and A. I. Duff, Thermodynamics up to the melting point in a TaVCrW high entropy alloy: Systematic *ab initio* study aided by machine learning potentials, Phys. Rev. B **105**, 214302 (2022).

[84] L. Dubrovinsky, N. Dubrovinskaia, O. Narygina, I. Kantor, A. Kuznetzov, V. B. Prakapenka, L. Vitos, B. Johansson, A. S. Mikhaylushkin, S. I. Simak, and I. A. Abrikosov, Body-centered cubic iron-nickel alloy in Earth's core, Science **316**, 1880 (2007).

[85] Y. Y. Ye, Y. Chen, K. M. Ho, B. N. Harmon, and P. A. Lindgard, Phonon-Phonon Coupling and the Stability of the High-Temperature bcc Phase of Zr, Phys. Rev. Lett. **58**, 1769 (1987).

[86] K. P. Migdal, P. A. Pokatashkin, and A. V. Yanilkin, Investigation of melting at the uranium γ phase by quantum and classical molecular dynamics methods, High Temp. **55**, 711 (2017).

[87] G. Kresse and J. Hafner, *Ab initio* molecular dynamics for liquid metals, Phys. Rev. B **47**, 558 (1993).

[88] G. Kresse and J. Hafner, *Ab initio* molecular-dynamics simulation of the liquid-metal–amorphous-semiconductor transition in germanium, Phys. Rev. B **49**, 14251 (1994).

[89] G. Kresse and J. Furthmüller, Efficient iterative schemes for *ab initio* total-energy calculations using a plane-wave basis set, Phys. Rev. B **54**, 11169 (1996).

[90] G. Kresse and J. Furthmüller, Efficiency of ab-initio total energy calculations for metals and semiconductors using a plane-wave basis set, Comput. Mater. Sci. **6**, 15 (1996).

[91] D. Knyazev and P. Levashov, *Ab initio* calculation of transport and optical properties of aluminum: Influence of simulation parameters, Comput. Mater. Sci. **79**, 817 (2013).

[92] S. Nosé, A unified formulation of the constant temperature molecular dynamics methods, J. Chem. Phys. **81**, 511 (1984).

[93] V. V. Kechin, Melting curve equations at high pressure, Phys. Rev. B **65**, 052102 (2001).

[94] D. Smirnova, S. Starikov, and I. Gordeev, Evaluation of the structure and properties for the high-temperature phase of zirconium from the atomistic simulations, Comput. Mater. Sci. **152**, 51 (2018).

[95] J. Gal, Cascading crystallographic transitions $\alpha \rightarrow \omega \rightarrow \beta \rightarrow \beta' \rightarrow \beta''$ and melting curve of elemental zirconium, Phys. B: Condens. Matter **613**, 412979 (2021).

[96] E. Stavrou, L. H. Yang, P. Söderlind, D. Aberg, H. B. Radousky, M. R. Armstrong, J. L. Belof, M. Kunz, E. Greenberg, V. B. Prakapenka, and D. A. Young, Anharmonicity-induced first-order isostructural phase transition of zirconium under pressure, Phys. Rev. B **98**, 220101(R) (2018).

[97] J. P. Perdew, K. Burke, and M. Ernzerhof, Generalized Gradient Approximation Made Simple, Phys. Rev. Lett. **77**, 3865 (1996).

[98] G. Kresse and D. Joubert, From ultrasoft pseudopotentials to the projector augmented-wave method, Phys. Rev. B **59**, 1758 (1999).

[99] Y. N. Ivashchenko and P. S. Martsenyuk, Measurement of the density of molten refractory metals, Ind. Lab. (USSR) (Engl. Transl.) **39**, 64 (1973).

[100] D. Steinberg, A simple relationship between the temperature dependence of the density of liquid metals and their boiling temperatures, Metall. Mater. Trans. B **5**, 1341 (1974).

[101] B. Allen, The surface tension of liquid transition metals at their melting points, Trans. AIME **227** (1963).

[102] C. Cagran, T. Hüpf, B. Wilthan, and G. Pottlacher, Selected thermophysical properties of Hf-3% Zr from 2200 K to 3500 K obtained by a fast pulse-heating technique, High Temp. - High Pressures **37**, 205 (2008).

[103] S. A. Kats, V. Ya. Chekhovskoi, and M. D. Kovalenko, Thermophysical properties of zirconium and hafnium at high temperatures, Teplofiz. Vys. Temp. **23**, 395 (1985).

[104] N. H. Paulson, E. Jennings, and M. Stan, Bayesian strategies for uncertainty quantification of the thermodynamic properties of materials, Int. J. Eng. Sci. **142**, 74 (2019).

[105] M. W. Chase, *NIST-JANAF Thermochemical Tables*, 4th ed. (American Institute of Physics for the National Institute of Standards and Technology, Washington, DC, 1998).

[106] I. Barin, O. Knacke, and O. Kubaschewski, *Thermochemical Properties of Inorganic Substances: Supplement* (Springer-Verlag, Berlin, Heidelberg, New York, 1977).

[107] L. V. Gurvich, I. V. Veits, and V. A. Medvedev, *Thermodynamic Properties of Individual Substances* (Nauka, Moscow, 1982), Vol. 4 (in Russian).

[108] G. V. Belov, S. A. Dyachkov, P. R. Levashov, I. V. Lomonosov, D. V. Minakov, I. V. Morozov, M. A. Sineva, and V. N. Smirnov, The IVTANTHERMO-Online database for thermodynamic properties of individual substances with web interface, J. Phys.: Conf. Ser. **946**, 012120 (2018).

[109] P. Lazor, G. Shen, and S. Saxena, Laser-heated diamond anvil cell experiments at high pressure: Melting curve of nickel up to 700 kbar, Phys. Chem. Miner. **20**, 86 (1993).

[110] S. Japel, B. Schwager, R. Boehler, and M. Ross, Melting of Copper and Nickel at High Pressure: The Role of *d* Electrons, Phys. Rev. Lett. **95**, 167801 (2005).

[111] D. Errandonea, High-pressure melting curves of the transition metals Cu, Ni, Pd, and Pt, Phys. Rev. B **87**, 054108 (2013).

[112] O. T. Lord, I. G. Wood, D. P. Dobson, L. Vočadlo, W. Wang, A. R. Thomson, E. T. H. Wann, G. Morard, M. Mezouar, and M. J. Walter, The melting curve of Ni to 1 Mbar, Earth Planet. Sci. Lett. **408**, 226 (2014).

[113] S. Boccato, R. Torchio, I. Kantor, G. Morard, S. Anzellini, R. Giampaoli, R. Briggs, A. Smareglia, T. Irifune, and S. Pascarelli, The melting curve of nickel up to 100 GPa explored by XAS, J. Geophys. Res.: Solid Earth **122**, 9921 (2017).

[114] R. Hrubiak, Y. Meng, and G. Shen, Microstructures define melting of molybdenum at high pressures, Nat. Commun. **8**, 14562 (2017).

[115] T. D. Cuong, N. Q. Hoc, N. D. Trung, N. T. Thao, and A. D. Phan, Theoretical predictions of melting behaviors of hcp iron up to 4000 GPa, Phys. Rev. B **106**, 094103 (2022).

[116] H. K. Hieu, Systematic prediction of high-pressure melting curves of transition metals, J. Appl. Phys. **116**, 163505 (2014).

[117] D. V. Minakov, M. A. Paramonov, and P. R. Levashov, *Ab initio* inspection of thermophysical experiments for molybdenum near melting, AIP Adv. **8**, 125012 (2018).

[118] D. V. Minakov, M. A. Paramonov, and P. R. Levashov, Thermophysical properties of liquid molybdenum in the near-critical region using quantum molecular dynamics, Phys. Rev. B **103**, 184204 (2021).

[119] D. V. Minakov, M. A. Paramonov, and P. R. Levashov, Interpretation of pulse-heating experiments for rhenium by quantum molecular dynamics, High Temp. - High Pressures **49**, 211 (2020).

[120] M. Boivineau and G. Pottlacher, Thermophysical properties of metals at very high temperatures obtained by dynamic heating techniques: Recent advances, Int. J. Mater. Prod. Technol. **26**, 217 (2006).

[121] D.-H. Kang, S. Jeon, H. Yoo, T. Ishikawa, J. T. Okada, P.-F. Paradis, and G. W. Lee, Nanosized nucleus-supercooled liquid interfacial free energy and thermophysical properties of early and late transition liquid metals, Cryst. Growth Des. **14**, 1103 (2014).

[122] D. M. Ceperley and B. J. Alder, Ground State of the Electron Gas by a Stochastic Method, Phys. Rev. Lett. **45**, 566 (1980).